Chapter 9 | Stellar warps

Abstract. In this Chapter we study stellar warp curves for a statistically complete sample of edge-on disk galaxies. We detect a warping feature on at least one side in 28 of our 44 sample galaxies ($\sim$ 64%). This implies that nearly all disk galaxies are warped, which means that stellar warps are long-lived, rather than transient.
From a detailed study of the differences between the B and I-band warp curves, we cannot confirm the hypothesis that *all* warps in the stellar disks of galaxies are caused by intergalactic magnetic fields or gas pressure, although these effects may play a role in a substantial fraction of our sample galaxies.
Gravitational interactions between neighbouring galaxies are not likely causes of *optical* warps. Instead, we argue that warps could be formed by the continuous infall of extragalactic material, which has not yet settled in the symmetry plane of the gravitational potential.
We find that the (projected) starting points of the stellar warps and the (major axis) B-band surface brightnesses at which the warps begin vary considerably among our sample galaxies.

1 Optical warps in edge-on disk galaxies

Many galaxies, including our own, show large-amplitude warps in the outer parts of their disks, although the degree and large-scale symmetry of the warping vary substantially among galaxies. Usually, warps are much more pronounced in HI observations than in the optical (e.g., Briggs, 1990; Binney, 1992), since they often begin near the edges of the stellar disks. For recent review articles about galaxy warps we refer the reader to Binney (1992) and Battaner (1995).

Although warps seem to be a gaseous feature of disk galaxies, stellar disks tend to follow the HI warps at their outer edges. Sasaki (1987) and Morrison et al. (1994) argue that the observation of a warping feature in NGC 5907 in a number of optical and near-infrared passbands implies that these warps are not merely gaseous, but also intrinsic to the *stellar* disks themselves.

Sánchez-Saavedra et al. (1990) claim that in almost half of the edge-on galaxies on the blue northern sky survey (POSS) plates and in about one third of them on the red POSS plates some sort of warping feature is observed. Battaner (1995) argues that existing observations of southern edge-on galaxies support this claim. Since optical warps can only be detected in edge-on disk galaxies if the line of nodes of the stellar warp lies relatively close to the direction perpendicular to line of sight, this implies that virtually all disk galaxies must be warped (e.g., Briggs, 1990). However, a corrugated dust lane can mimic the presence of an optical warp (Bottema, 1996).

Additional problems can arise if a galaxy is not completely edge-on, since projected spiral arms may resemble a warping feature; on the other hand, a warp in the stellar distribution may also be hidden due to projection effects.

1.1 The stellar warp in our Galaxy

The tracers used in most studies of an optical counterpart of the HI warp in the Galaxy (e.g., Djorgovski & Sosin, 1989, and references therein; Porcel & Battaner, 1995) are young, with ages generally smaller than a Galactic rotation period, and could therefore have formed in the warp itself, near their present locations. For that reason one cannot draw firm conclusions on the Galactic warp's longevity and persistence from the distribution of its young optical tracers. Moreover, optical studies of the young disk tracers are severely hampered by the interstellar extinction and by incompleteness effects.

Based on the *IRAS* observations, Djorgovski & Sosin (1989) concluded that the *old* stellar population in the Galaxy follows the HI warp, although not exactly. This indicates that the Galactic warp is a feature of the Galaxy as a whole and not merely of the gaseous component (Djorgovski & Sosin, 1989).

The observation that the Galactic warp is traced by a relatively old, evolved stellar population (of AGB and post-AGB stars) implies that it is a long-lived phenomenon: the life times of AGB stars in the range of the observed IRAS luminosities are on the order of a few times 10^9 years (Aaronson & Mould, 1985).

Although the Galactic warp traced by the evolved stellar population does not trace the HI warp exactly, it seems that the optical warp defined by the (young) OB associations is equal or even stronger than the gaseous warp. Porcel & Battaner (1995) interpret this observation as a result of Galactic extinction, since low-Galactic latitude stars are discriminated against in the selection of distant young tracers.

1.2 Colour gradients in galaxy warps

1.2.1 Colour gradients as a diagnostic tool

If warps are gravity-induced, the stellar and gaseous warps should behave similarly, because gravity affects stars and gas in the same way. However, if warps are caused by magnetic fields or intergalactic gas pressure, the gas layer is expected to respond more strongly to the forces exerted upon the disk than the stellar component.

Therefore, the comparison between the stellar warps in blue and red passbands of a statistically complete sample of southern edge-on disk galaxies that we make in this Chapter can help to distinguish between the possible formation mechanisms. Ideally, one would compare observations done in different optical passbands, representative of various stellar populations, as well as HI observations, which trace the gas component.

In a number of warping edge-on galaxies, for which observations with high spatial resolution of the outer parts are available, it is found that, although the stellar warps generally follow the HI warps in the same direction, the spatial differences are appreciable (e.g., Jensen & Thuan, 1982; Sasaki, 1987; Florido et al., 1991). Florido et al. (1991) found, in a number of highly-inclined disk galaxies, a wavelength dependence in the sense that the bluest colours (representing the youngest stellar populations) showed the largest deviations from the galaxy planes, similar to the observations of the Galactic warp.

They argue that these differences cannot be caused by extinction (e.g., Sasaki, 1987), since extinction will reduce the actual separation between warps observed in the gaseous component, the young and the old stellar populations. Therefore, intrinsic colour gradients will be reduced rather than emphasized by extinction effects.

However, optical warp curves are generally defined by the loci of maximum intensity along a galaxy's major axis. The presence of a corrugating central dust lane can greatly hamper the determination of such a warp curve, and essentially mimic an optical warp. This effect is strongest in the bluer passbands, where the effects of dust are most noticeable.

Alternatively, it has been proposed that warps are excited by a discrete bending mode in a sharply truncated galaxy disk (e.g., Hunter & Toomre, 1969; Sparke & Casertano, 1988; and others). Due to the gaseous viscosity it can then be expected that the warp curves determined from the gas layer and younger stars (that will have formed recently from the interstellar gas), will be slightly offset from warp curves based on emission from the older stellar populations, since these are not as much governed by viscous processes.

However, if the disk mass is not sharply truncated, the warp will exhibit a continuum of bending modes and cannot be maintained sufficiently long because of differential precession (e.g., Hunter & Toomre, 1969; and others). If a disk which shows a continuum of bending modes is somehow forced to warp, the outer regions will warp strongly, because the only way to dissipate the energy carried outwards by the bending waves is by the vertical heating of the disk. Then, this outer strongly warped region will rapidly dissipate its energy and hence the warp will be dissolved quickly (Sparke & Casertano, 1988). If the outer edge is sufficiently sharp, however, the bending wave can be reflected and a stable warp may form.

1.2.2 The effects of a sharp disk truncation

The discrepancy between the observed spatial positions of the stellar and gaseous warps could be explained by invoking projection effects rather than a physical separation between the stars and the gas layer. Because of the sharp truncation of the stellar disk observed in a number of edge-on galaxies (e.g., van der Kruit & Searle, 1981a,b, 1982a,b), the stellar warp appears weaker than the HI warp (e.g., Sasaki, 1987; Freudenreich et al., 1994). Such a projection effect can occur if the direction of the maximum vertical displacement of the stellar disk differs from the line of nodes and if the stellar disk is much smaller than the gaseous one.

Porcel et al. (1997) point out that the discrepancy between the Galactic HI warp and the optical warp curve based on the *DIRBE* experiment, flown on board *COBE*, argues in favour of a cut-off of the Galactic stellar disk at about $R = 15$ kpc, which is in agreement with the results of Ruphy et al. (1996).

Cox et al. (1996), on the other hand, did not find any evidence for a spatial separation between the optical and HI warps in NGC 7170. In view of the absence of a sharp truncation of the stellar disk and because the HI gas extends only slightly further out than the stellar disk, it is indeed expected that these projection effects do not occur.

Stellar and gaseous warps thus seem to be very similar.

1.2.3 Spatial differences

If the warp is induced by an external force to which the stars respond differently than the gas, a deviation between the stellar and gaseous warps is foreseen. Intergalactic magnetic fields or intergalactic gas pressure, for instance, would primarily act on the gaseous galaxy components, so that any warp resulting from such external forces will be at first a gaseous distortion. A stellar warp would follow due to subsequent star formation in the gaseous warp. However, although the young stars will trace the gaseous warp closely, the older stars would have had time to return to the original galaxy plane, or to disperse their warped distribution (Florido et al., 1991).

Battaner et al. (1990, 1991) argued that intergalactic magnetic fields of order 10^{-6} to 10^{-8} G can produce warps in the gaseous disks of galaxies and that a uniform intergalactic magnetic field can actually explain the observed warps within about 20 Mpc of the Galaxy, including the warps of the Galaxy, M31 and M33. Although Binney (1991) rejects this mechanism, arguing that implausibly high field strengths are required to account for the observed warps, Battaner (1995 and priv. comm.) points out that very large intergalactic magnetic fields on order of the required 1–3 μG seem to be ubiquitous (see, e.g., Kronberg, 1994).

However, the determination of intrinsic colour gradients perpendicular to the galaxies' major axes is not at all straightforward, as we will discuss in Sect. 2.

1.3 Outline of the present analysis

In this Chapter we study the frequency, wavelength dependence and global properties of stellar warps, based on observations of a statistically complete sample of edge-on disk galaxies. We will describe the sample characteristics and our reduction strategy in Sect. 2. In Sect. 3 we present the results of our analysis of optical warps. Implications of these results are discussed in Sect. 4. Finally, Sect. 5 summarizes our results and conclusions.

2 Approach

In Chapter 2 we described the selection of our sample of highly-inclined disk galaxies, the observations, and the reduction techniques applied to our observational data. We will confine ourselves here to summarize the selection criteria that were applied to the galaxies contained in the Surface Photometry Catalogue of the ESO-Uppsala Galaxies (ESO-LV; Lauberts & Valentijn, 1989):

- their inclinations are greater than or equal to 87°;
- the angular blue diameters (D^B_{25}) are larger than 2.′2;
- the galaxy types range from S0 to Sd, and
- they should be non-interacting and undisturbed.

To study the colour dependence of the warp of a given galaxy, one needs to treat the observations using standardized procedures. Therefore, we identify the position along the

galaxy's major axis and the direction perpendicular to the galaxy plane by x and z, respectively. In this reference frame, the *warp curve* of a given galaxy is defined by positions (x_i, z_i), which are representative of the warping of the galaxy with respect to the galaxy's symmetry plane at a given distance from the galactic centre $(x_i, z_i) = (0, 0)$, projected onto the plane of the sky.

We will summarize the main steps that have to be taken to obtain reliable warp curves (see also Jiménez-Vicente et al., 1997):

- First, we have to make sure that foreground stars will not contaminate the final curve;
- Then, we determine the warp curve by extrapolating the essentially dust-free outer galaxy profiles (i.e., at high z distances) inwards. To determine the geometric centres we applied an intensity-weighted algorithm to the regions with surface brightnesses between 24.0 and 27.0 B-mag arcsec^{-2}, which corresponds to a range between, roughly, 22.5 and 25.5 I-mag arcsec^{-2} (depending on the B–I colours of the sample galaxies). The resulting curves are more robust to the disturbing influence of dust than a warp curve based on the loci of maximum intensity (obtained from Gaussian fits), which are very sensitive to the effects of a strong central dust lane. In the radially outer regions, where optical warps are expected to be found, both methods yield identical results, however.
- Finally, the central 3 (I-band) scale lengths of the galaxy were used to rotate the image so that this part of the galaxy coincided with the x axis. This step is crucial to obtain a reliable curve; special care has to be taken when dealing with dusty galaxies. For each galaxy we used the I-band observations to determine the rotation angle, so as to be least affected by dust contamination. The same rotation angle was then applied to the B-band images.

Since optical warps generally occur at the faintest surface brightness levels, where the signal-to-noise ratios are small, the resulting curves are extremely sensitive to disturbing effects of either foreground stars or a corrugating dust lane, as we will show in Sect. 3.1.

In general, our B-band images trace the galaxy disks further out than the I-band observations. However, in the B band the contamination by interstellar dust seriously affects the resulting curves, even in the outermost disk regions (see Sect. 3.1). The application of an unsharp masking technique to enhance low-surface brightness structures proved to be limited by the noise in our images; by determining the warp curves from the original observations, we could trace the galaxy disks further out. To enhance the signal-to-noise ratio in the outer parts, we applied a radial binning algorithm to the resulting warp curves. Generally, we are able trace the galaxy light out to 27.5–28.0 B-mag arcsec^{-2}.

3 Analysis of optical warps

3.1 Frequency and colour dependence of stellar warps

In Sect. 2 we described the method we used to determine the warp curves. The results of this exercise are presented in Fig. 1. The upper panels show the B-band warp curve; the lower panels indicate the differences between the B and I-band curves.

In this figure, all features on larger scales than the small-scale noise features are real structures. For the purposes of this Chapter, we classify those galaxies of which the outer parts of the (mean levels of the) curves deviate from the mean galaxy plane by more than twice the intrinsic noise in the curves, as possible candidates to exhibit optical warps. However, these deviations do not necessarily represent stellar warps or corrugations of the galaxy disks. Especially in the inner regions, the deviations from the mean galaxy planes are often caused by dust contamination. This is reflected by the differences between the B and I-band curves for a number of our sample galaxies (Fig. 1, lower panels).

De Vaucouleurs (1958) already pointed out that an integral-sign warp could also be a manifestation of the outward decrease of intensity along the galaxy's major axis coupled with obscuration effects. To assess the importance of these effects, we used B–I colour maps as dust indicators. In a significant fraction of our sample galaxies, the B–I colour maps showed clear evidence that the contamination by dust is not negligible, even in the outer disk regions, where stellar warps are expected to be detectable.

As we already showed in de Grijs et al. (1997, Chapter 8), the effects of interstellar dust are characterized by significantly redder colours, which are generally confined to a well-defined central dust lane. These central dust lanes exhibit steep vertical colour gradients on either side, leveling off towards a flat and nearly featureless colour of the main (old) disk component. We excluded those galaxies that exhibited clear dust signatures from the analysis in the remaining part of this Chapter (see Table 1), based on the combined information derived from both the individual B and I images and the B–I colour maps. In Fig. 2 we present calibrated B–I colour maps for our sample galaxies, from which one can estimate the importance of dust in the outer regions and that of actively star forming regions along the spiral arms, if a galaxy is not seen exactly edge-on.

From the rather homogeneous and very blue colour distributions in the outer parts of the remaining sample galaxies for which we detected warping features we conclude that the effects of dust are small or negligible.

Moreover, deviations from the mean galaxy planes may also be due to the contributions of actively star forming regions, e.g., in the spiral arms. Therefore, a non-negligible deviation from an inclination of 90° may result in a "warped" appearance. This effect is particularly obvious in ESO 202-G35 (panel 9) and ESO 286-G18 (panel 15), both in the original observations *and* in the B–I colour maps. Because of these unpredictable effects of dust extinction combined with a non-negligible deviation from an inclination of 90°, we left these two galaxies out of the analysis as well.

In many cases, we can trace the stellar disk further out in the B band than in the I band. This is reflected by the radially outwards decreasing signal-to-noise ratios in a number of the difference profiles in Fig. 1 (lower panels). Therefore, we decided to study the behaviour of the outer regions of the stellar disks of our sample galaxies in the B band. Table 1 gives an overview of the results we obtained for our sample galaxies.

From the results presented in Table 1 we point out that in at least 13 out of our 44 sample galaxies ($\sim$ 30%) a two-sided warping feature can be discerned. In 15 more galaxies, we detect a deviation from the plane on one side (either because

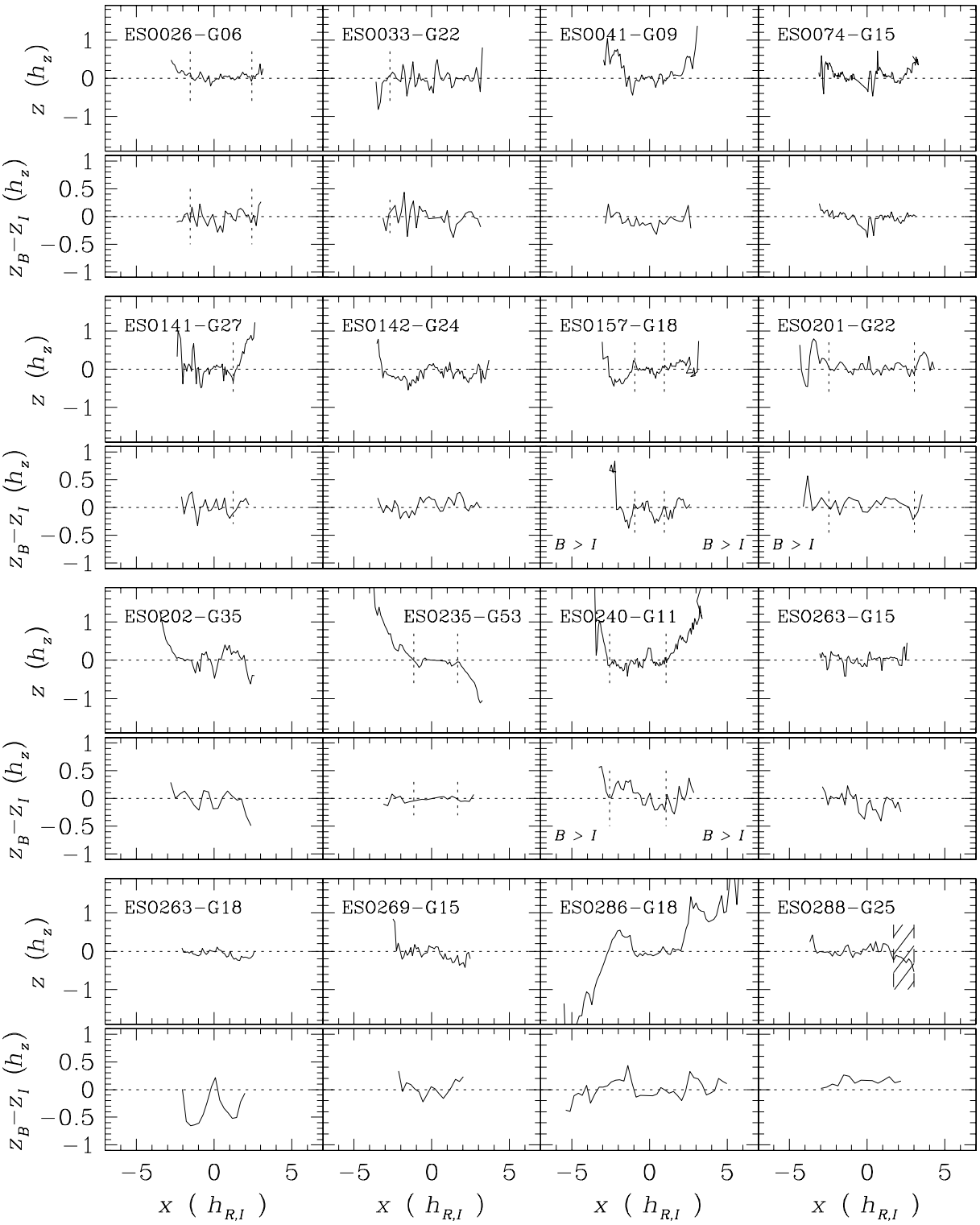

Fig. 1. Warp curves of our sample galaxies. The upper panels show the B-band warp curves; the lower panels show the spatial differences between the warp curves in B and I (data points are binned in bins of $\sim 3''$ to reduce the noise in the curves); significant and systematic spatial differences are indicated in these panels. The dotted lines in the upper panels indicate the starting points of the warps, $R_{\rm warp}$; the hatched regions have been excluded from the analysis because of contamination by foreground stars.

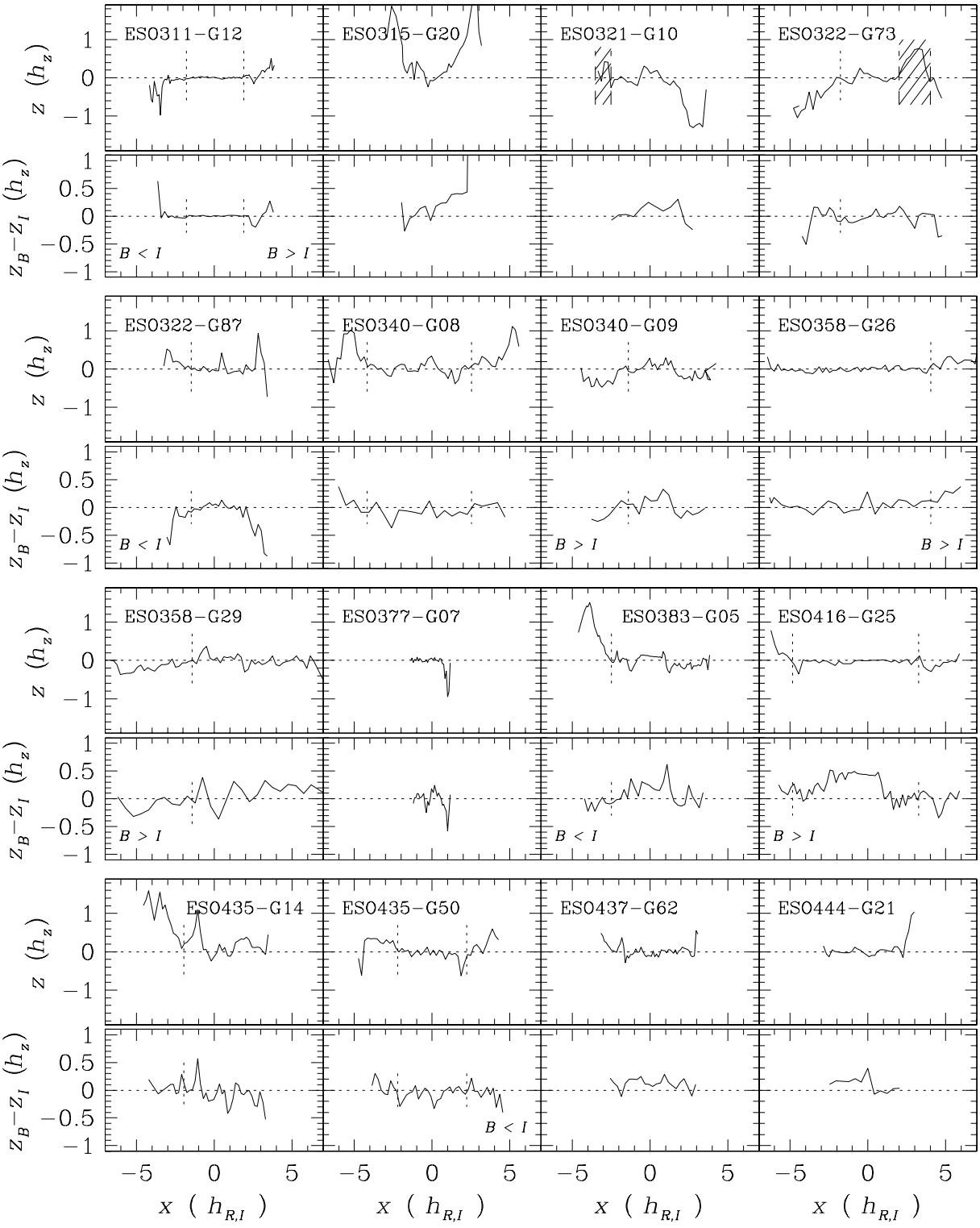

Fig. 1. (Continued)

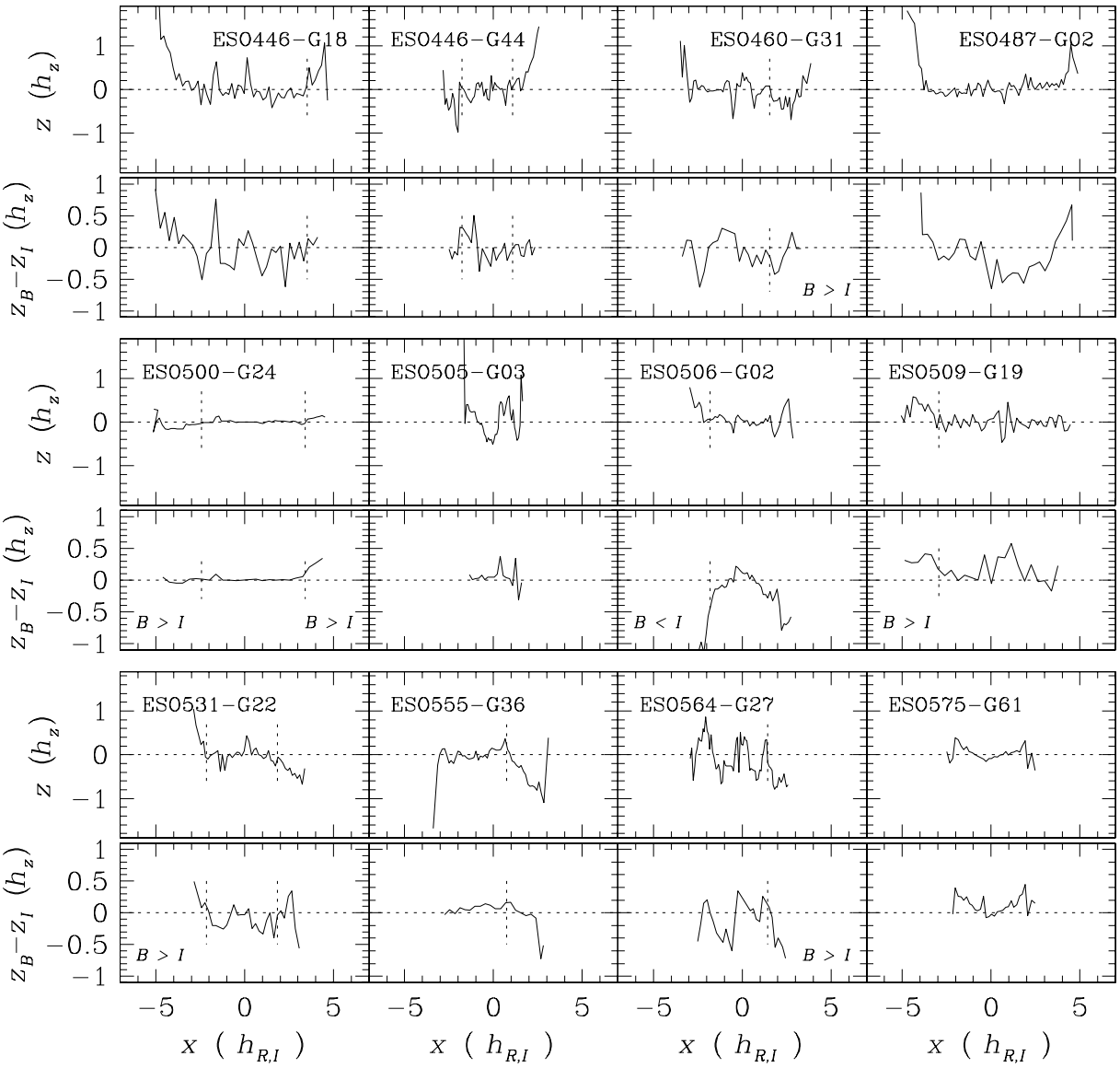

Fig. 1. (Continued)

of dust contamination or a superposed foreground star on the other side, or because of the absence of a warping feature on that side), at least down to the surface brightness levels that we can reach with our observations. Therefore, the main result of this analysis is that we detect a warping feature on at least one side in 28 of our 44 sample galaxies ($\sim$ 64%). The statistical error in this warp frequency equals 4 (or 9%), under the assumption of a binomial distribution of warps in galaxies. Based on the original B and I-band images and the B–I colour maps, we are confident that these warping features were caused neither by inclination nor by dust effects These results are consistent with those obtained by Sánchez-Saavedra et al. (1990), who claim to have detected optical warps in 42 out of 86 of their galaxies ($\sim$ 49%) on the blue POSS plates. This agreement is remarkably good considering the difference in determination methods (Sánchez-Saavedra et al. (1990) obtained their frequency by examining their sample galaxies by eye). Similar claims have been published for galaxy warps detected in HI 21cm observations (e.g., Bosma & Athanassoula, 1990).

Sánchez-Saavedra et al. (1990) discussed the implications of such a high frequency of *observed* optical warps in edge-on disk galaxies for the *actual* frequency of warps in stellar disks. They argued that the angle between the line of nodes of the optical warp and the line of sight should be at least 34 to 37° so as to be observable. Therefore, one should multiply the observed frequency of optical warps by 1.65 ± 0.05 to obtain the actual number of warped stellar disks. These calculations are consistent with the hypothesis that nearly all disk galaxies are warped. Although the optical warp frequency of 83%

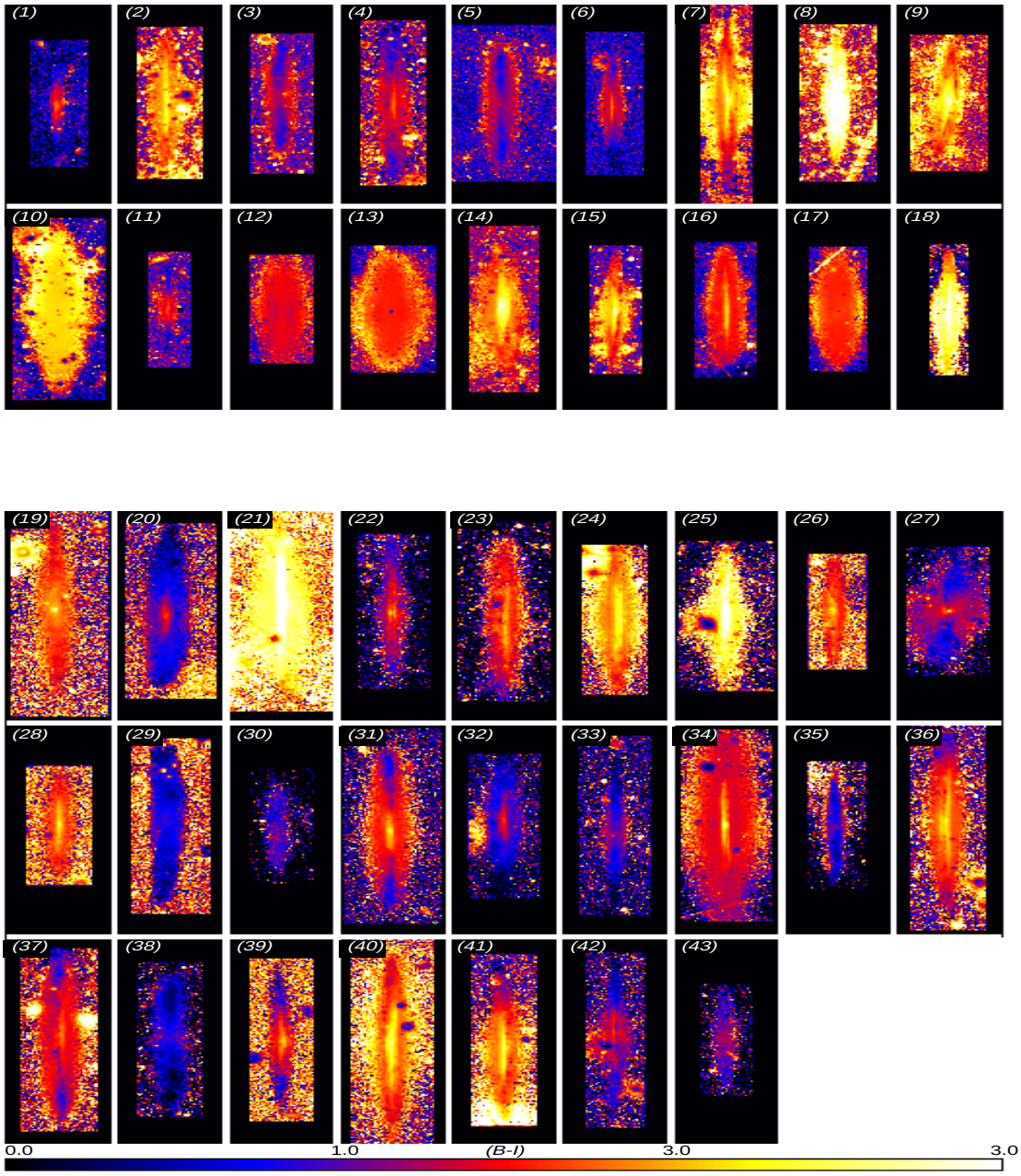

Fig. 2. Calibrated *B–I* colour maps of our sample galaxies. Maps *(1)* – *(18)* and *(19)* – *(43)* are displayed on the same scale. Maps *(1)* – *(18)* have been inserted in rectangular frames of size $120'' \times 330''$; maps *(19)* – *(43)* in frames of $60'' \times 180''$. Galaxy images were rotated from their original sky orientations so that the major axes lie vertically, corresponding to negative to positive galactocentric distances from top to bottom (see Fig. 1).
(1) ESO033-G22; *(2)* ESO041-G09; *(3)* ESO141-G27; *(4)* ESO142-G24; *(5)* ESO157-G18; *(6)* ESO201-G22; *(7)* ESO240-G11; *(8)* ESO263-G15; *(9)* ESO286-G18; *(10)* ESO311-G12; *(11)* ESO340-G08; *(12)* ESO358-G26; *(13)* ESO358-G29; *(14)* ESO383-G05; *(15)* ESO460-G31; *(16)* ESO487-G02; *(17)* ESO500-G24; *(18)* ESO564-G27; *(19)* ESO026-G06; *(20)* ESO202-G35; *(21)* ESO235-G53; *(22)* ESO263-G18; *(23)* ESO269-G15; *(24)* ESO288-G25; *(25)* ESO315-G20; *(26)* ESO321-G10; *(27)* ESO322-G73; *(28)* ESO322-G87; *(29)* ESO340-G09; *(30)* ESO377-G07; *(31)* ESO416-G25; *(32)* ESO435-G14; *(33)* ESO435-G50; *(34)* ESO437-G62; *(35)* ESO444-G21; *(36)* ESO446-G18; *(37)* ESO446-G44; *(38)* ESO505-G03; *(39)* ESO506-G02; *(40)* ESO509-G19; *(41)* ESO531-G22; *(42)* ESO555-G36; *(43)* ESO575-G61.

quoted by Sánches-Saavedra et al. (1990) should be treated with caution, due to the small-number statistics involved, it is indeed indicative of the high frequency of warped galaxy disks, expected from HI observations.

In view of the hypothesis that warps are induced by intergalactic magnetic fields or gas pressure, a detailed study of the differences between the B and I-band warp curves is of interest.

We wish to determine the spatial offsets between the B and I-band warp curves, if any, from a detailed study of Fig. 1 (lower panels). We tried to do so by binning the B and I-band warp curves with different (radial) bin sizes, to determine any *systematic* differences, which were not introduced by the binning procedure. A significant and systematic spatial difference is appreciated if, *at radii beyond* $R_{\rm warp}$, the ratio of the number of data points sampled in bins of $\sim 1''$ (i.e., a size comparable to the spatial resolution limit) one either side of the locus of equality (where $z_B - z_I = 0$ in Fig. 1) exceeds 1.15, thus allowing for an intrinsic scatter of 15%.

From Table 1, we already determined 41 possible warping features, in 28 of our 44 sample galaxies. In 21 out of these 41 cases ($\sim$ 51%), we could not determine any significant deviation of the B-band from the I-band warp curve, either because of the noisy warp curves, or because of a close match between the warp curves obtained in either passband. Such a close match may be obtained if the stellar populations traced by the blue and red colours are spatially coincident or by an overall effect of dust extinction, forcing the colours to match. Of the remaining 20 warping features, 15 ($\sim$ 37% of the 44 sample galaxies) showed a significantly and *systematically* greater deviation from the galaxy plane in the B band than in the I band, whereas the other 5 ($\sim$ 12%) showed the opposite behaviour (as indicated in the lower panels of Fig. 1). This behaviour is also reflected by the *vertical* colour gradients in the warping regions that one can distinguish in the B–I colour maps. We will discuss the spatial differences between the warps defined by the B and I-band emission in detail for the prominently warping galaxy ESO235-G53 (Sect. 3.3).

The spatial differences between the B and I-band curves of the other galaxies, that were not included in this statistical analysis, can generally be attributed to the non-negligible effects of dust extinction.

If warps were magnetically induced, one would expect that the young and old stellar populations in a galaxy disk, traced by the B and I-band light, are systematically displaced with respect to each other, in the sense that the B-band warp would deviate further from the average galaxy plane than the I-band warp. However, it is as yet unknown by how much the B-band warps are expected to deviate from the I-band warps, since we do not know the fraction of young stars that contribute to the I-band luminosity (Battaner, priv. comm.), nor the precise dependence of the warp strength on passband, in the sense that we do not know how representative the B and I bands are as tracers of very young and very old stellar populations, respectively.

Although we cannot confirm the hypothesis that galaxy warps are, *in general*, caused by intergalactic magnetic fields, since only part of the observed warps show a behaviour like the one expected if they were magnetically induced, in a significant fraction of our sample galaxies magnetic fields (or intergalactic gas pressure) may play a significant role, since to date no other physical processes are known that can account for spatial differences between red and blue warps.

3.2 Correlations of optical warps with global galaxy properties

Although warps have been detected in both the gaseous and the stellar disks of the majority of disk galaxies, the precise conditions for their presence are yet unknown. In this section we will study possible correlations between the presence of optical warps in our sample galaxies and global galaxy characteristics.

In Fig. 3 we show the detected frequency of optical warps as a function of galaxy type, for both our sample galaxies and the sample of Sánchez-Saavedra et al. (1990). Since we are dealing with small-numbers statistics, we can only conclude that there is no obvious trend with type; this result is confirmed by the observations of Sánchez-Saavedra et al. (1990). One should note that the frequencies we present in this figure are lower limits. The optical warp frequencies we find are systematically higher than those quoted by Sánchez-Saavedra et al. (1990). Even though the numbers of galaxies studied are small, this effect is likely due to the nature of our samples. Since Sánchez-Saavedra et al. (1990) studied all northern-hemisphere NGC spiral galaxies with $\log R_{25} \geq 0.57$, they included galaxies in their sample that are less highly-inclined than our sample galaxies. As argued in Sect. 1, a deviation of even a few degrees from an inclination of 90° may hide an optical warp due to projection effects and thus result in a lower frequency of detected optical warps.

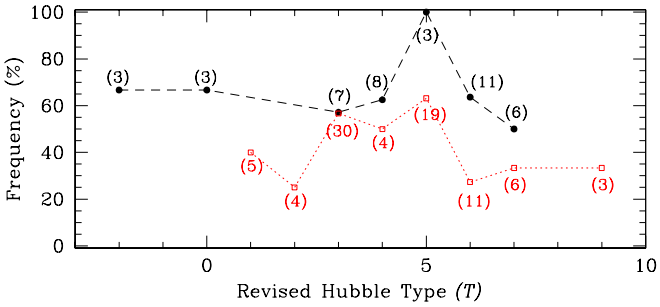

Fig. 3. Type dependence of the detected optical warps in both our sample galaxies (dashed line) and the sample of Sánchez-Saavedra et al. (1990, dotted line). The numbers indicate the total number of sample galaxies on which the frequencies are based.

We also investigated whether the occurrence of (optical) warps is related to the extent of the galaxy disks, indicated by their maximum rotation velocity (taken from Mathewson et al., 1992). However, we did not detect any statistically significant differences between galaxies with low or high rotation velocities, nor between compact and extended galaxies (as indicated by their scale lengths).

In Table 1 we present the global properties of the warps that we detected in our sample galaxies. The accuracy of our determinations is indicated by the error estimates.

In order to quantify the optical warps, we first define the warp starting point, $R_{\rm warp}$, as the radius where the average levels of the curves start deviating *systematically* from the

Table 1. Optical warps and warp parameters

Columns: (1) Galaxy name (the numbers correspond to the panels in Fig. 1); (2)–(9) Warp parameters on one side of the galaxy; and (10)–(17) on the other side (*corr.* = corrugated plane; *dust* = detection impossible due to dust; *incl.* = inclination $\neq 90°$; *star* = detection impossible due to superposed foreground star). Columns (4)–(5) and (12)–(13) tabulate the starting point of the warp and the measurement error (in I-band scale lengths); (6) and (14) B-band surface brightness at $R_{\rm warp}$, on the major axis (B-mag arcsec^{-2}; typical errors are 0.05–0.10 B-mag arcsec^{-2}); (7)–(8) and (15)–(16) warp strength in B and I (see text; the errors are of order 15%); (9) and (17) B-band warp angle (see text).

Galaxy	Side	Warp	$R_{\rm warp}$	$\pm$	$\mu_{B,\rm warp}$	$z_{\rm max}/\ell_{\rm warp}$		$\alpha_{\rm warp}$	Side	Warp	$R_{\rm warp}$	$\pm$	$\mu_{B,\rm warp}$	$z_{\rm max}/\ell_{\rm warp}$		$\alpha_{\rm warp}$
(ESO-LV)			($h_{R,I}$)			(B)	(I)	(°)			($h_{R,I}$)			(B)	(I)	(°)
(1)	(2)	(3)	(4)	(5)	(6)	(7)	(8)	(9)	(10)	(11)	(12)	(13)	(14)	(15)	(16)	(17)
026-G06	W	+	1.54	0.13	23.51	0.048	0.059	2.8	E	+	2.44	0.13	24.62	0.149	0.049	8.5
033-G22	N	+	2.69	0.15	24.23	–0.107	–0.090	6.1	S	–	—	—	—	—	—	—
041-G09	NE	dust	—	—	—	—	—	—	SW	dust	—	—	—	—	—	—
074-G15	NE	corr.	—	—	—	—	—	—	SW	corr.	—	—	—	—	—	—
141-G27	NE	–	—	—	—	—	—	—	SW	+	1.24	0.09	22.00	0.105	0.079	6.0
142-G24	N	dust	—	—	—	—	—	—	S	–	—	—	—	—	—	—
157-G18	N	+	0.94	0.11	21.25	–0.048	–0.053	2.8	S	+	0.94	0.07	21.50	0.029	0.030	1.7
201-G22	NE	+	2.46	0.08	22.59	0.107	0.065	6.1	SW	+	3.03	0.08	22.95	0.100	—	5.7
202-G35	NW	incl.	—	—	—	—	—	—	SE	incl.	—	—	—	—	—	—
235-G53	NE	+	1.15	0.14	23.23	0.145	0.137	8.2	SW	+	1.66	0.07	23.43	–0.193	–0.182	10.9
240-G11	NE	+	2.57	0.07	23.63	0.199	0.126	11.3	SW	+	1.06	0.05	22.43	0.050	0.044	2.9
263-G15	W	–	—	—	—	—	—	—	E	–	—	—	—	—	—	—
263-G18	NW	dust	—	—	—	—	—	—	SE	dust	—	—	—	—	—	—
269-G15	N	dust	—	—	—	—	—	—	S	dust	—	—	—	—	—	—
286-G18	NE	incl.	—	—	—	—	—	—	SW	incl.	—	—	—	—	—	—
288-G25	NE	dust	—	—	—	—	—	—	SW	star	—	—	—	—	—	—
311-G12	N	+	1.79	0.06	21.95	–0.061	–0.034	3.5	S	+	1.90	0.06	22.23	0.045	0.021	2.6
315-G20	NE	dust	—	—	—	—	—	—	SW	dust	—	—	—	—	—	—
321-G10	NE	star	—	—	—	—	—	—	SW	dust	—	—	—	—	—	—
322-G73	NE	+	1.76	0.15	21.14	–0.117	–0.047	6.7	SW	star	—	—	—	—	—	—
322-G87	NW	+	1.49	0.11	21.57	0.088	0.049	5.0	SE	–	—	—	—	—	—	—
340-G08	NE	+	4.18	0.19	24.39	0.111	0.125	6.4	SW	+	2.53	0.19	23.18	0.057	0.071	3.3
340-G09	W	dust	—	—	—	—	—	—	E	+	1.40	0.25	21.84	–0.049	—	2.8
358-G26	W	–	—	—	—	—	—	—	E	+	4.04	0.26	22.61	0.057	—	3.3
358-G29	NW	+	1.43	0.20	20.13	–0.042	–0.042	2.4	SE	–	—	—	—	—	—	—
377-G07	NW	–	—	—	—	—	—	—	SE	–	—	—	—	—	—	—
383-G05	NW	+	2.49	0.09	23.77	0.282	0.262	15.7	SE	–	—	—	—	—	—	—
416-G25	N	+	4.84	0.30	22.09	0.178	0.053	10.1	S	+	3.25	0.15	22.58	–0.066	—	3.8
435-G14	NE	+	1.94	0.15	21.20	0.087	0.038	5.0	SW	–	—	—	—	—	—	—
435-G50	W	+	2.23	0.12	23.10	0.024	0.037	1.4	E	+	2.23	0.12	22.85	0.044	0.038	2.5
437-G62	N	–	—	—	—	—	—	—	S	–	—	—	—	—	—	—
444-G21	NW	–	—	—	—	—	—	—	SE	–	—	—	—	—	—	—
446-G18	N	+	3.51	0.10	23.51	0.128	0.222	7.3	S	dust	—	—	—	—	—	—
446-G44	W	+	1.77	0.06	22.22	–0.058	—	3.3	E	+	1.07	0.09	21.76	0.081	0.082	4.6
460-G31	W	dust	—	—	—	—	—	—	E	+	1.54	0.10	23.51	–0.036	–0.090	2.0
487-G02	NE	dust	—	—	—	—	—	—	SW	dust	—	—	—	—	—	—
500-G24	NE	+	2.44	0.10	21.73	–0.020	–0.019	1.2	SW	+	3.42	0.10	22.87	0.036	—	2.0
505-G03	NW	+[1]							SE	+[1]						
506-G02	N	+	1.81	0.08	22.37	0.085	0.079	4.9	S	–	—	—	—	—	—	—
509-G19	NE	+	2.93	0.20	23.09	0.091	—	5.2	SW	–	—	—	—	—	—	—
531-G22	N	+	2.14	0.12	23.02	0.166	0.122	9.4	S	+	1.83	0.16	22.46	–0.039	–0.051	2.3
555-G36	NW	–	—	—	—	—	—	—	SE	+	0.74	0.15	23.22	–0.079	–0.044	4.5
564-G27	N	–	—	—	—	—	—	—	S	+	1.43	0.04	24.03	–0.074	—	4.2
575-G61	N	–	—	—	—	—	—	—	S	–	—	—	—	—	—	—

NOTE:

[1] ESO 505-G03 is completely curved; it is therefore not possible to determine global warp parameters unambiguously.

mean galaxy planes. Since we have already binned the warp curves of Fig. 1 radially (in bins of $\sim 3''$) the warp curves consist of independent data points. Therefore, if the mean level of a particular warp curve starts to deviate from the average galaxy plane (defined by the emission in the inner 3 I-band scale lengths), as reflected by the increasingly larger deviation in a number of subsequent data points, the deviation represents a real variation in the mean galaxy plane, and its starting point is called the warp radius, $R_{\rm warp}$. In Fig. 1 we have indicated the warp radii by vertical dotted lines.

To compare our results, obtained from optical warp curves, to warps detected in HI 21cm observations, only a small number of sufficiently detailed studies are available in the literature. From a study of the extended HI distribution in a sample of 12 disk galaxies, Briggs (1990) concluded that the HI layer is typically flat within $\mu_B = 25$ mag arcsec^{-2}, whereas warping becomes detectable within the Holmberg radius, where $\mu_{\rm Ho} = 26.5$ B-mag arcsec^{-2}. If we assume that Freeman's (1970) result holds for these galaxies, i.e., the central surface brightness of galaxy disks $\mu_{0,B} = 21.65 \pm 0.3$ mag arcsec^{-2}, this means that the HI warps generally start between 3.2 and 4.6 scale lengths. However, ideally one should compare warp starting points that were determined in exactly the same way. From Fig. 5 of Cox et al. (1996), we estimate that the HI warp in NGC 7170 starts between 50 and $60''$, depending on the galaxy's side, which corresponds to $R_{\rm warp} = 1.6 - 1.9$ R-band scale lengths. Similarly, as was shown by Jiménez-Vicente et al. (1997), based on Bottema's (1995) observations of NGC 4013 and using a similar definition of $R_{\rm warp}$ as we did, the HI warp of this galaxy starts at 6.07 kpc, which corresponds to $R_{\rm warp} = 2.6$ F-band scale lengths (using $h_{R,F} = 2.3$ kpc [$H_0 = 75$ km s^{-1} Mpc^{-1}]; Bottema, 1995). These results are comparable to ours.

It is well-known that the Galactic warp starts at about 12 kpc from the Galactic centre (e.g., Burton, 1988). Since it is generally agreed upon that the scale length of the Galactic disk is ~ 3 kpc (see, e.g., Sackett, 1997), this means that $R_{\rm warp,Gal} \approx 4.0 h_{R,\rm true}$, which is slightly further out than the radii we found, on average. However, we based our results on the I-band scale lengths, which are likely larger than the "true" disk scale lengths (due to dust; see, e.g., de Grijs et al., 1997 [Chapter 8]; Chapter 5). Therefore, our results and those obtained for our Galaxy also appear to be comparable.

We also need the surface brightness in the galaxy plane at the warp radius, $\mu_{\rm warp}$, and its (dimensionless) strength for a detailed description of the warp. We define the warp strength as the quotient of the maximum excursion of the stellar layer out of the galaxy plane (irrespective of the detailed warp shape), $z_{\rm max}$, and the (projected) warp length, $\ell_{\rm warp} = R(z_{\rm max}) - R_{\rm warp}$. Due to the complex and noisy warp curves, the errors in the values for the warp strength are on the order of 15%. In some cases we could not determine the I-band warp strength due to the noise in the warp curves. Note that the projected warp length is a function of the angle between the line of nodes and the line of sight; detailed kinematic observations are needed to disentangle the effects of projection, however. In fact, the warp strength is a measure of the warp angle, $\alpha_{\rm warp} = \arctan(z_{\rm max}/\ell_{\rm warp})$, which is also tabulated in Table 1. In some cases the warp curves back to the galaxy plane after having reached its maximum deviation in one hemisphere. This behaviour is not accounted for in our global description of the optical warps in our sample.

Although the differences between the B and I-band warp strengths should be treated with caution due to the noise in the warp curves, they do reflect the trend in spatial differences between the B and I-band warp curves noticed in Sect. 3.1.

3.3 The warping galaxy ESO 235-G53

3.3.1 Global characteristics

The most prominent warp that we detected among our sample galaxies is exhibited by the Sb galaxy ESO 235-G53. Although ESO 235-G53 is a member of a well-defined group of galaxies (Maia et al., 1989) it does not seem to be affected by gravitational interaction with any of the other group members. In fact, Buta & Crocker (1993) claimed that only one other group member, ESO 235-G58, appears obviously distorted (based on the SRC-J southern sky survey plates), whereas they failed to notice the prominent optical warp in ESO 235-G53.

In this section we will study the characteristics of the optical warp of this galaxy in detail. Unfortunately, the determination of the precise starting points of the optical warp on either side is hampered by the presence of bright foreground stars, in particular on the northeastern side. The B-band warp curve of ESO 235-G53 is presented in Fig. 4*a*; we have (linearly) interpolated the regions affected by the foreground stars.

If one rotates the B-band image by 180°, it appears that the overall warp structure is slightly asymmetric, which is reflected by the difference in starting points: on the northeastern side the warp starts at $1.15 \pm 0.14 h_{R,I}$, whereas the deviation from the mean plane on the southwestern side begins at $1.66 \pm 0.07 h_{R,I}$.

3.3.2 Colour dependence

In Fig. 4*b* we show the spatial differences between the B and I-band warp curves of ESO 235-G53. From a detailed examination of this figure, we cannot conclude that the B and I-band warps are significantly displaced with respect to each other, although one might argue that a spatial difference is appreciated in the warp regions, in the sense that the I-band warp is stronger than the warp in the B band; this effect is independent of the radial binning that was applied. We will discuss this observation in more detail in Sect. 4.2.

On the other hand, the warp regions exhibit a clear radial colour dependence. Fig. 4*c* shows the behaviour of the B–I colour along the warp curve.

One can immediately see that the warp regions are characterized by a significantly different colour with respect to the main galaxy disk: the colour difference is of order 0.5 mag. This effect cannot be entirely due to the absence of interstellar dust, since a comparison between the colours at large z distances (which are supposed to be relatively dust free; see, e.g., de Grijs et al., 1997 [Chapter 8]) and those in the warp regions shows that they also exhibit a significant colour gradient (although smaller). A similar colour gradient is found in the other sample galaxies.

In the inner regions, the relatively blue colour along the warp curve is most likely due to a line-of-sight effect, in the sense that we predominantly observe the outer disk stars (in front of a dusty disk), which may also be intrinsically bluer than the inner disk stars (although they do not need to be much bluer, since the contamination by dust will likely dominate the observed colours). At intermediate radii the colours

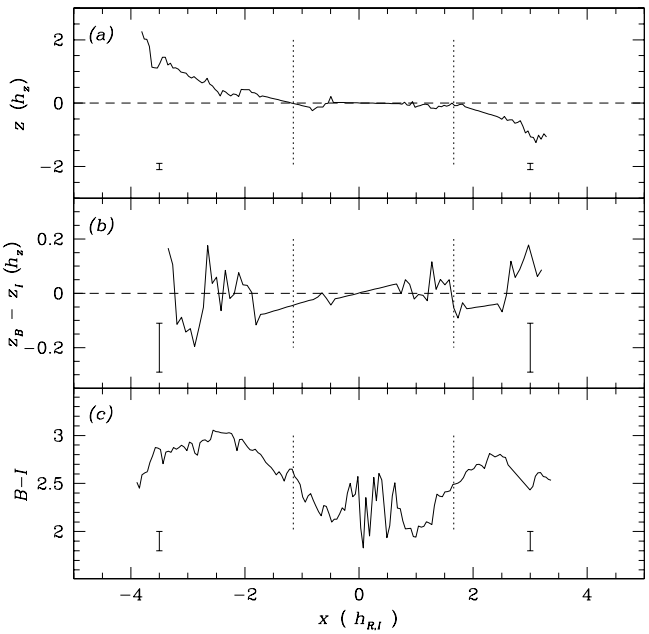

Fig. 4. *(a)* B-band warp curve of ESO 235-G53 (northeast is to the left, southwest to the right); *(b)* Spatial differences between the B and I-band warp curves of ESO 235-G53; *(c)* B–I colours along the warp curve. The dotted lines indicate the estimated warp starting points, $R_{\rm warp}$, on either side. Typical errors are indicated by the error bars in the outer regions. The featureless regions close to the warp starting points, and extending into the warp regions, in panels *(a)* and *(b)* are the result of the interpolation that was needed because of bright foreground stars.

become increasingly redder, which is likely caused by the increasingly dominant effects of dust extinction and the less dominant contribution to the overall light contribution by the outermost, unobscured disk stars. Finally, the increasingly blue colours in the warp regions are most likely due to the (near) absence of a large amount of dust at those galactocentric distances, perhaps combined with relatively recent star formation in the outer disk (warp) regions.

4 Discussion

4.1 The frequency of optical warps

Based on geometrical arguments, the observed frequency of $\sim 64\%$ of stellar galaxy disks that exhibit some kind of warping feature at their outer edges, is consistent with an actual frequency of warped disks close to 100% (Sect. 3.1). This frequency is comparable to the frequency of warped gaseous disks, based on HI 21cm observations (e.g., Bosma & Athanassoula, 1990). This implies that these phenomena are long-lived, rather than transient.

Sánchez-Saavedra et al. (1990) showed that projection effects cause optical warps to become invisible rapidly if the angle between the line of nodes and the line of sight decreases to below $\sim 34°$. However, one might be able to detect a warping stellar disk for even smaller angles by examining the behaviour of the dust layer (e.g., Steiman-Cameron et al., 1992). On the other hand, a warping dust layer does not necessarily represent the stellar distribution closely, but may be tilted with respect to the stellar symmetry plane (Steiman-Cameron et al., 1992). Therefore, one should treat conclusions based on the dust distribution in a galaxy disk with due caution.

Finally, if a galaxy is not completely edge-on, projected spiral arms may resemble a warping feature; on the other hand, a warp in the stellar distribution may also be hidden due to such inclination effects.

4.2 Formation mechanisms

To date, a physically realistic mechanism to account for both the formation and the persistence of warps in disk galaxies, either stellar or gaseous, has not yet been found. All mechanisms postulated suffer from incompleteness or the inability to explain the warping stellar and gaseous features in detail. However, due to the large number of unknown variables, the solution of this problem is not straightforward. Moreover, due to the complexity of the physical processes involved, in calculations one often simplifies reality and thus introduces large uncertainties (e.g., Binney, 1992).

Of the various warp formation and sustaining processes that have been proposed, the magnetic field or gas pressure induced warping mechanism could be tested observationally with the data set presented in this Chapter. If warps were magnetically induced, one would expect the younger stars, represented by the bluest emission, to be warping more strongly than the older stellar populations, traced by the redder galaxy light. Also, one would expect this effect to become more noticeable in the more strongly warped galaxies.

From a detailed study of the spatial differences between the B and I-band warp curves in ESO 235-G53 (Sect. 3.3), the galaxy in our sample that exhibits the most prominent warp, we found that a spatial difference, if any, suggests a more strongly warped appearance in the I band compared to the B-band warp curve, although our results are consistent with no spatial difference at all.

We investigated a possible dependence of the sense of the spatial differences between the B and I-band warp curves on their environment. If warps are magnetically induced, or due to intergalactic gas pressure, one would expect the deviations to be stronger in clusters than in the field, as the intracluster magnetic fields are likely stronger than the intercluster fields (e.g., Kronberg, 1994). Again, the expected spatial differences would be in the sense that the B-band warps are stronger than those detected in the I band. However, we did not find any such correlation among the warps exhibited by our sample galaxies. This does not necessarily mean that warps cannot be produced by magnetic fields or intergalactic gas pressure, since these effects may also be sufficiently strong and effective both in the field and in galaxy clusters.

However, as already noted in Sect. 3.1, based on the statistics of the deviations between the B and I-band warp curves, we cannot confirm the hypothesis that galaxy warps are, *in general*, caused by intergalactic magnetic fields, although they may play a significant role in a fair number of our sample galaxies.

The increasingly blue colour with galactocentric distance that we find in all our sample galaxies indicates that the dominant stellar population in the warp regions is relatively

younger and thus has undergone active star formation more recently than the dominant stellar population in the main disk. If this age difference is somehow related to the warp formation, neither magnetic fields nor intergalactic gas pressure are likely formation processes.

Instead, one could argue that warps are formed by the continuous infall of extragalactic material (e.g., gas-rich dwarf galaxies in the halo), which has not yet settled in the symmetry plane of the gravitational potential. This continuous supply of infalling mass will cause a redistribution of the halo angular momentum, which in turn could sustain the warping disk (e.g., Bottema, 1995). Stars will have formed from the infalling gas relatively more recently than the dominant stellar population in the main disk, thus causing bluer warp colours.

In the context of the Cold Dark Matter cosmogony galaxies are formed by accretion and mergers of smaller lumps of matter (e.g., Ostriker & Binney, 1989). It is therefore expected that this process of "secondary infall" in the outer galactic haloes is still ongoing. However, this process can only explain one-sided warps (Bottema, 1996) or otherwise irregular warps. It takes a few galactic rotation periods for a gas cloud that has been accreted to regularize into a symmetric structure.

One may wonder if the infall of extragalactic material will eventually destroy the main galaxy disk. From numerical calculations, Quinn et al. (1993) conclude that the effects of so-called "minor mergers", i.e., the accretion of a smaller object by a disk galaxy, can be to produce structural features like the flaring of the main disk (e.g., de Grijs & Peletier, 1997 [Chapter 7]) and its warping. They conclude that even a single merger of a disk galaxy and a satellite is sufficient to destroy a thin disk, even if the mass of the satellite is relatively small compared to that of the disk galaxy. Warps are formed because of the redistribution of the disk and satellite mass, which is driven by the conservation of angular momentum.

These results should be treated with caution, however (e.g., Walker et al., 1996), since this study had the draw-back of not being fully self-consistent: Quinn et al. (1993) used a rigid, non-responsive dark halo, in which the resulting warp could be maintained for at least 10 rotation periods before being destroyed by differential precession. In a live, responsive halo the persistence of a stellar warp is much more difficult to accomplish (e.g., Dubinski & Kuijken, 1994; Nelson & Tremaine, 1995).

In Table 2 we give an overview of the possible group membership of our sample galaxies, based on the available evidence in the literature. It seems unlikely that all warps in our sample galaxies are induced by gravitational interaction with neighbouring galaxies: 21 of our 44 sample galaxies are obvious field galaxies without nearby neighbours, neither optically nor spatially. Of these 21 isolated galaxies, 12 exhibit a clear warping feature on at least one side, whereas only 3 of them do not. This is consistent with evidence based on HI 21cm observations that many isolated field galaxies show prominent warps (e.g., Sancisi, 1976; Cox et al., 1996).

Moreover, in a number of the remaining galaxies we detect a symmetrical warp, which is hard to produce by means of gravitational interaction, due to the time needed for a warp to regularize globally (e.g., Burton, 1988). Some of them may be genuine field galaxies as well, since in many cases their cluster or group membership is based only on optical coincidences.

4.3 Warp characteristics and projection effects

For 8 out of the 28 warping galaxies in our sample we showed that the warp curve, after reaching a maximum amplitude in one hemisphere, returns to the galaxy plane and may end in the opposite hemisphere (see Fig. 1). Several mechanisms could cause this effect: it may be due to either projection effects or to an intrinsic physical mechanism. Projection effects include a non-negligible angle between the line of nodes of the warp and the direction perpendicular to the line of sight, and the contribution of emission from a spiral arm that is seen not completely edge-on. If the latter projection effect were important, one should reduce the frequency of observed optical warps to $\sim 45\%$, as opposed to the $\sim 64\%$ quoted in Sect. 3.1. Even so, the actual frequency of warped stellar disks would still be high ($\sim 75\%$) and comparable to the frequency of warps detected in HI 21cm observations. Note that these warp frequencies of $\sim 45\%$ (or $\sim 75\%$) should be treated as lower limits!

On the other hand, the effect may also be caused by contamination by a prominent dust lane, or reflect a physical corrugation of the galaxy disk, similar to the warp in our Galaxy.

As we can conclude from Table 1, the (projected) starting points of the stellar warps we detected ($R_{\rm warp,proj}$, expressed in I-band scale lengths, $h_{R,I}$) vary considerably among our sample galaxies ($\langle R_{\rm warp}\rangle = 2.1 \pm 1.0 h_{R,I}$). Even if the stellar warps in all our sample galaxies would begin at more or less the same radius, such an effect could be expected due to the projection of the line of nodes onto the plane of the sky. The projected starting point of the warp is thus a function of the angle between the line of sight and the line of nodes of the warp. If the lower limit to this angle is $\sim 34^\circ$ (Sánchez-Saavedra et al., 1990), it follows from simple geometric arguments that the projected warp starting points vary between $R_{\rm warp,proj} \approx 0.56 R_{\rm warp}$ and $R_{\rm warp}$, with $\langle R_{\rm warp,proj}\rangle \approx 0.78 R_{\rm warp}$.

If the conditions for optical warps can be compared to those governing HI warps, one could argue that, in general, warps are expected to start at approximately the same (projected) galactocentric distance. This argument is based on the observation that in a fair number of galaxies the HI warp starts at the edge of the stellar disk (e.g., Sancisi, 1983; Bottema, 1995), where the disk material is less tightly bound by the galaxy's gravitational potential. This is likely also true for the stars at the edges of the galaxy disks. Combined with the observations and arguments in favour of a disk truncation radius at an approximately constant number of disk scale lengths (van der Kruit & Searle, 1981a,b, 1982a,b; Barteldrees & Dettmar, 1993), this leads to the suggestion that $R_{\rm warp} \approx$ constant. However, if this were the case, it would be difficult to explain the observation that in a fair number of our sample galaxies that exhibit two-sided warps the starting points on either side are not symmetric with respect to the galaxy centre.

From the optical observations alone we cannot infer the precise distribution of the angles between the line of sight and the lines of node of our sample galaxies, unless we assume that all warps start at exactly the same galactocentric distance. One needs kinematic data with high spatial and velocity resolution, in particular in the outer parts of the galaxies, to be able to do so.

Table 2. Group membership of the sample galaxies

Columns: (1) Galaxy name (ESO-LV); (2) and (3) Indication whether the disk is warped and if the warp occurs on (at least) one or both sides; (4) redshift; (5) Nearest neighbours; this list contains all known neighbouring galaxies within 8.′0 (15.′0 if their velocities are known), as well as all group or cluster centres within 15.′0 (References: *BCS89*: Bothun et al., 1989; *DCL86*: Dickens et al., 1986; *MdL89*: Maia et al., 1989; *R87*: Richter, 1987; *S96*: Stein, 1996); (6) distance from sample galaxy in arcsec; (7) redshift; (8) Field galaxy or cluster member (References: *ESO U*: Lauberts, 1982; *SGC*: Corwin et al., 1985)

Galaxy (ESO-LV) (1)	Warp (2)	1/2-sided (3)	Redshift (z) (4)	Nearest neighbours (5)	Distance (arcmin) (6)	Redshift (z) (7)	Field/cluster (F/C) (8)
026-G06	+	2	0.00917	—			F
033-G22	+	1	0.01460	—			F
041-G09	?		0.01473	—			F
074-G15	?		0.00199	ESO 074-IG 20	14.8	0.03700	F
141-G27	+	1	0.00614	—			F
142-G24	?		0.00643	—			C (ESO U)
157-G18	+	2	0.00453	APMBGC 157+052+052	1.8	not available	C (ESO U)
				Dorado group (centre)	13.9	0.00310	
201-G22	+	2	0.01357	APMBGC 201–065–069	4.7	not available	F
202-G35	?		0.00616	Abell 3271 (centre)	11.5	not available	F
235-G53	+	2	0.01715	ESO 235-IG 52	4.4	not available	C (ESO U)
				NGC 7014 group (centre)	5.2	0.01629	
				ESO 235-IG 48	6.7	not available	
240-G11	+	2	0.00960	[MdL89] 30	7.1	not available	C (ESO U)
				IRAS F23349–4807	7.1	not available	
				ESO 240-G 10	13.5	0.01101	
263-G15	–		0.00843	—			F
263-G18	?		not available	ESO 263-G 19	6.1	0.01404	C (ESO U)
269-G15	?		0.01135	NGC 4835	11.7	0.00731	F
286-G18	?		0.03051	ESO 286-G 17	1.5	0.03262	interacting pair
				Abell 3723 (centre)	7.5	not available	
288-G25	?		0.00829	AM 2156-441	6.3	not available	C (ESO U, NGC 7162)
311-G12	+	2	0.00377	—			F
315-G20	?		0.01615	IRAS 09404–4142	7.7	0.01630	C (ESO U)
321-G10	?		0.01050	—			F
322-G73	+	≥ 1	0.01097	[BCS89] 028	1.4	not available	C (ESO U)
				[BCS89] 029	5.7	not available	
				NGC 4677	10.7	0.01049	
				NGC 4696A	14.6	0.00873	
322-G87	+	1	0.01212	[BCS89] 046	2.4	not available	C (ESO U)
				[DCL86] 214	6.4	0.01201	
				NGC 4696E	8.3	0.00615	
				PGC 043268	13.3	0.01357	
				ESO 322-G 85	13.5	0.01322	
340-G08	+	2	0.00946	ESO 340-G 10	12.9	not available	C (ESO U)
340-G09	+	≥ 1	0.00870	—			F
358-G26	+	1	0.00540	FCCB 1024	2.6	not available	C (ESO U)
				FCCB 1006	4.0	not available	
				FCCB 1035	6.0	not available	
				Abell 3138 (centre)	6.8	not available	
				FCCB 0980	7.2	not available	
				FCCB 1040	7.6	not available	
				FCCB 0985	7.7	not available	
				LGG 096 group (centre)	13.4	not available	
358-G29	+	1	0.00575	FCC 168	5.3	not available	C (ESO U, Fornax I)
				FCC 171	5.4	not available	
				FCCB 1075	6.0	not available	
				FCCB 1102	6.0	not available	
				FLSBG 248	6.5	not available	
				MCG -06-09-008	6.6	0.00608	
				FCC 160	7.9	not available	
				NGC 1380B	9.7	0.00601	
				NGC 1379	10.4	0.00460	

Table 2. (Continued)

Galaxy (ESO-LV) (1)	Warp (2)	1/2-sided (3)	Redshift (z) (4)	Nearest neighbours (5)	Distance (arcmin) (6)	Redshift (z) (7)	Field/cluster (F/C) (8)
				NGC 1387	13.6	0.00434	
				RSCG 24 group (centre)	13.8	0.00500	
377-G07	–		not available	ESO 377-G 06	3.5	not available	C (ESO U)
383-G05	+	1	0.01213	—			F
416-G25	+	2	0.01664	Abell S0301:[S96] 002	9.1	0.10458	C (ESO U)
				Abell S0301:[S96] 003	9.3	0.10487	
				APMBGC 416–062+097	10.4	0.02327	
				Abell S0301:[S96] 004	12.5	0.10454	
				Abell S0301:[S96] 006	13.4	0.10321	
435-G14	+	1	0.00888	ESO 435-G 16	14.7	0.00307	C (ESO U)
435-G50	+	2	0.00908	—			C (ESO U)
437-G62	–		0.00941	—			F
444-G21	–		0.01420	[R87] 088	4.3	0.01334	C (ESO U)
				CL 1322-30:[S96] 003	10.1	0.17297	
				CL 1322-30:[S96] 002	12.8	0.01349	
				CL 1322-30:[S96] 004	12.9	0.01456	
				IRAS 13202-2938	13.2	0.03400	
				CL 1322-30:[S96] 005	14.4	0.01223	
446-G18	+	≥ 1	0.01577	—			F
446-G44	+	2	0.00921	—			F
460-G31	+	≥ 1	0.01921	—			F
487-G02	?		0.00585	ESO 487-G 03	8.6	not available	F
500-G24	+	2	0.00809	ESO 500-G 23	3.1	not available	C (ESO U)
505-G03	+	2	0.00603	UGCA 261	12.1	0.00569	paired/cluster
				LGG 265 group (centre)	13.5	not available	
506-G02	+	1	0.01321	IC 3152	9.0	0.01113	optical pair (SGC)
509-G19	+	1	0.03554	ESO 509-G 24	5.7	0.04351	F
531-G22	+	2	0.01134	—			F
555-G36	+	1	not available	—			C (SGC)
564-G27	+	1	0.00726	—			F
575-G61	–		0.00552	ESO 575-G 60	5.7	not available	C (ESO U/SGC)

It appears that there is no clear correlation between the warps' starting points, $R_{\rm warp}$, and their strengths, $z_{\rm max}/\ell_{\rm warp}$.

4.4 Warps from a near-infrared perspective

In the previous section we noticed that the average, projected warp starting point, $\langle R_{\rm warp,proj}\rangle$, turned out to be 2.1 ± 1.0 $h_{R,I}$, with a rather large spread around the mean value. These observed small warp radii (in terms of the I-band scale lengths) might imply that one could circumvent the problems caused by dust extinction by studying the disks of edge-on galaxies at near-infrared wavelengths, where it is much more difficult than in the optical to trace the galaxy disks out to large galactocentric distances.

From a comparison between the values for $R_{\rm warp}$ presented in Table 1 and Fig. 6 of de Grijs et al. (1997, Chapter 8), which is indicative of the extent of the disks of our sample galaxies in the K-band, one can see that our it K-band observations do not always (or just) reach the radii at which the optical warps become detectable. This is particularly clear if one realises that the outermost data points in that figure were obtained from significantly (radially) binned vertical surface brightness profiles, in order to increase the signal-to-noise ratios at those galactocentric distances. If one wishes to detect optical warps, however, one should avoid any radial binning exceeding $\sim 1.''5 - 2.''0$. Therefore, we can study the K-band behaviour of our galaxy disks in the regions where the optical warps were detected only in a few cases.

In this section we will study in detail the B and K-band structure, and in particular the spatial differences between the B and K-band warp curves, in three of our sample galaxies that exhibit warping features in the optical passbands: ESO 311-G12 ($T = 0.0$), ESO 358-G29 ($T = -1.6$), and ESO 446-G44 ($T = 6.0$). Fig. 5 shows the data we will base the analysis on; for each of the three sample galaxies we present the B and K-band warp curves, and their spatial difference profiles. In addition, we show the spatial difference profiles between the B and I-band warp curves (see Fig. 1) on the same scale as that between B and K.

In Sect. 2 we described our method to determine the B and I-band warp curves. The K-band warp curves for these three sample galaxies are based on the equivalent B-band regions, using the average $B-K$ galaxy colours away from the galaxy planes: for ESO 311-G12, $B - K \simeq 4.5$, for ESO 358-G29, $B - K \simeq 3.5$, and for ESO 446-G44, $B - K \simeq 4.0$.

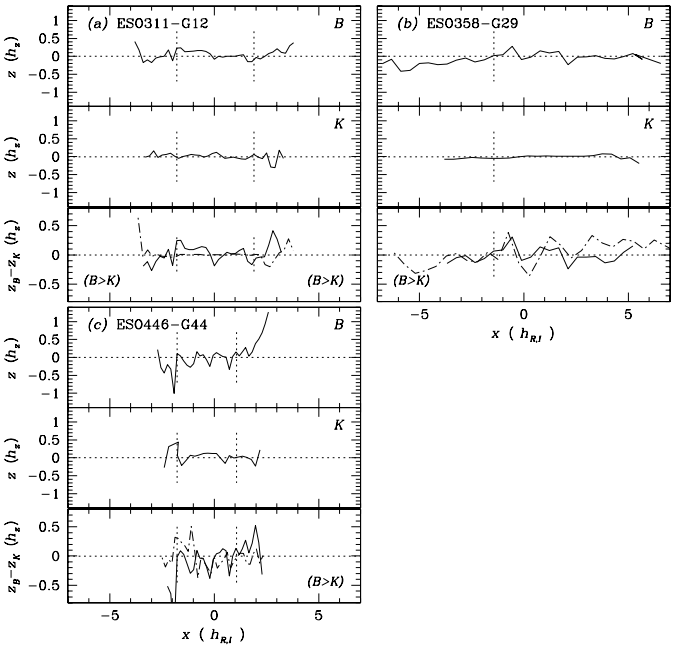

Fig. 5. B and K-band warp curves, and their spatial difference profiles for *(a)* ESO 311-G12, *(b)* ESO 358-G29, and *(c)* ESO 446-G44. The dotted lines indicate the estimated warp starting points (obtained from the B-band observations), $R_{\rm warp}$, on either side; the sense of the spatial differences, if significant, has been indicated in the lower panels, for each galaxy. The dash-dotted lines in the lower panels show the spatial difference profiles between the B and I-band warp curves, taken from Fig. 1.

Although our K-band warp curves do not trace the galaxy disks as far out as the B-band curves, due to the short exposure times used to obtain our K-band observations, the detailed examination of the spatial difference curves shows that the comparison between our B and K-band observations confirms our conclusions drawn in Sect. 3.1, based on the study of the spatial differences between the B and I-band warp curves. A comparison between the spatial difference curves for these three sample galaxies between B and K and between B and I shows that the spatial differences between the B and K-band warp curves are more pronounced than between B and I, whereas the K-band warp curves basically do not exhibit warping features, as opposed to the optical warp curves. However, one should be careful when comparing the spatial difference profiles, since our K-band observations do not trace the disks as far out as the optical data.

The spatial differences between the warp curves derived from the optical and near-infrared observations of our sample galaxies could be caused by the contribution to the emission by actively star forming regions, that are more prominent in the optical (bluer) passbands than in the near-infrared.

Therefore, a detailed study of stellar warp curves both in the optical and at near-infrared wavelengths appears to open up promising perspectives. Thus, ideally one should obtain deeper observations in the K band, in order to study spatial differences between the warp curves over a longer wavelength range, and thus a greater age range. Moreover, the effects of dust can thus be minimized.

5 Summary and Conclusions

In this Chapter we have presented B-band warp curves for our sample galaxies. From careful examination of these warp curves, we obtained the following main observational results and conclusions:

- We detect a warping feature on at least one side in 28 of our 44 sample galaxies ($\sim$ 64%). Based on geometrical arguments (e.g., Sánchez-Saavedra et al., 1990), this frequency of observed optical warps is consistent with the hypothesis that nearly all disk galaxies are warped. Such a high frequency implies that these phenomena are long-lived, rather than transient.
- We did not find any obvious correlations between the occurrence of optical warps and galaxy type, size (indicated by the rotation velocity) or compactness (based on the galaxies' radial scale lengths).
- One should be cautious in interpreting optical warp curves. Contamination by dust or projected spiral arms (if a galaxy is not completely edge-on) may resemble a warping feature; on the other hand, a warp in the stellar distribution may also be hidden due to such inclination effects.
- From a detailed study of the differences between the B and I-band warp curves, we cannot confirm the hypothesis that *all* galaxy warps are caused by intergalactic magnetic fields or gas pressure, although these processes may play a significant role in a fair number of our sample galaxies. Since a large fraction of our field galaxies exhibit some kind of warping feature, and because a number of the possible cluster members show a regular two-sided warp, gravitational interaction between neighbouring galaxies is, in general, not likely to be the cause of optical warps.
  Instead, if the observed colour gradients along the galaxies' major axes are somehow related to the warp formation process, one could argue that warps are formed by the continuous infall of extragalactic material, which has not yet settled in the symmetry plane of the gravitational potential.
- The (projected) starting points of the stellar warps, $R_{\rm warp,proj}$, and the (major axis) B-band surface brightnesses at which the warps begin vary considerably among our sample galaxies. This could be either an intrinsic characteristic of the galaxy disks, or due to projection effects. The starting points of the warps and their strengths do not exhibit any correlation.
- From a study of the spatial differences between the B and K-band warp curves for three of our sample galaxies, we argue that ideally one should obtain deeper observations in the K band, so that one can study spatial differences between the warp curves over a longer wavelength range, and thus a greater age range. Moreover, the effects of dust can thus be minimized. A comparison between the spatial difference profiles of a small number of our sample galaxies between the warp curves in the B and K bands and those between the B and I-band warp curves suggests that the spatial differences between the B and K-band warp curves are more pronounced than those between the B and I-band

curves, whereas the K-band warp curves basically do not exhibit warping features.

Acknowledgements I would like to thank the Departamento de Física Teórica y del Cosmos of the Universidad de Granada (Spain), in particular Eduardo Battaner and Jorge Jiménez-Vicente, for their hospitality during a working visit in April 1997, when the analysis presented in this Chapter was initiated. Discussions with Frank Briggs, Koen Kuijken, Reynier Peletier, Renzo Sancisi and Roelof Bottema have greatly stimulated this work. This research has made use of the NASA/IPAC Extragalactic Database (NED) which is operated by the Jet Propulsion Laboratory, California Institute of Technology, under contract with the National Aeronautics and Space Administration (NASA).

References

Aaronson, M., Mould, J., 1985, ApJ 288, 551

Barteldrees, A., Dettmar, R.-J., 1993, A&AS 103, 475

Battaner, E., 1995, in: The Formation of the Milky Way, eds. Alfaro, E., Tenorio-Tagle, G., Cambridge: Cambridge Univ. Press, p. 77

Battaner, E., Florido, E., Sánchez-Saavedra, M.-L., 1990, A&A 236, 1

Battaner, E., Florido, E., Sánchez-Saavedra, M.-L., Prieto, M., 1991, in: Warped Disks and Inclined Rings Around Galaxies, eds. Casertano, S., Sackett, P.D., Briggs, F.H., Cambridge: Cambridge Univ. Press, p. 200

Binney, J.J., 1991, in: Dynamics of Disk Galaxies, ed. Sundelius, B., Göteborg: Dept. Astron., Chalmers Univ., p. 297

Binney, J.J., 1992, ARA&A 30, 51

Bosma, A., Athanassoula, E., 1990, in: Dynamics and Interactions of Galaxies, ed. Wielen, R., Berlin: Springer, p. 356

Bothun, G.D., Caldwell, N., Schombert, J.M., 1989, AJ 98, 1542

Bottema, R., Shostak, G.S., van der Kruit, P.C., 1987, Nature 328, 401

Bottema, R., 1995, A&A 295, 605

Bottema, R., 1996, A&A 306, 345

Briggs, F.H., 1990, ApJ 352, 15

Burton, W.B., 1988, in: Galactic and Extragalactic Radio Astronomy, eds. Verschuur, G.L., Kellermann, K.I., New York: Springer, p. 295

Buta, R., Crocker, D.A., 1993, AJ 106, 939

Corwin, H. G. Jr., de Vaucouleurs, A., de Vaucouleurs, G., Southern Galaxy Catalogue, 1985, Austin: University of Texas **(SGC)**

Cox, A.L., Sparke, L.S., van Moorsel, G., Shaw, M., 1996, AJ 111, 1505

de Grijs, R., Peletier, R.F., 1997, A&A 320, L21 **(Chapter 7)**

de Grijs, R., Peletier, R.F., van der Kruit, P.C., 1997, A&A, in press **(Chapter 8)**

de Vaucouleurs, G., 1958, ApJ 127, 487

Dickens, R.J., Currie, M.J., Lucey, J.R., 1986, MNRAS 220, 679

Djorgovski, S., Sosin, C., 1989, ApJ 341, L13

Dubinski, J., Kuijken, K., 1995, ApJ 442, 492

Florido, E., Prieto, M., Battaner, E., Mediavilla, E., Sánchez-Saavedra, M.-L., 1991, A&A 242, 301

Freeman, K.C., 1970, ApJ 160, 811

Freudenreich, H.T., Berriman, G.T., Dwek, E., Hauser, M.G., Kelsall, T., Moseley, S.H., Silverberg, R.F., Sodroski, T.J., Toller, G.N., Weiland, J.L., 1994, ApJ 429, L69

Hunter, C., Toomre, A., 1969, ApJ 155, 747

Jensen, E.B., Thuan, T.X., 1982, ApJS 50, 421

Jiménez-Vicente, J., Porcel, C., Sánchez-Saavedra, M.-L., Battaner, E., 1997, ApSS, in press

Kronberg, P.P., 1994, Rep. Progress in Physics, 57:4, 325

Lauberts, A., The ESO/Uppsala Survey of the ESO(B) Atlas, 1982, ESO **(ESO U)**

Lauberts A., Valentijn, E.A., 1989, The Surface Photometry Catalogue of the ESO-Uppsala Galaxies, ESO **(ESO-LV)**

Maia, M.A.G., da Costa, L.N., Latham, D.W., 1989, ApJS 69, 809

Mathewson, D.S., Ford, V.L., Buchhorn, M., 1992, ApJS 81, 413

Morrison, H.L., Boroson, T.A., Harding, P., 1994, AJ 108, 1191

Nelson, R.W., Tremaine, S., 1995, MNRAS, 275, 897

Ostriker, E.C., Binney, J.J., 1989, MNRAS 237, 785

Porcel, C., Battaner, E., 1995, MNRAS 274, 1153

Porcel, C., Battaner, E., Jiménez-Vicente, J., 1997, A&A 322, 103

Quinn, P.J., Hernquist, L., Fullagar, D.P., 1993, ApJ 403, 74

Richter, O.-G., 1987, A&AS 67, 261

Ruphy, S., Robin, A.C., Epchtein, N., Copet, E., Bertin, E., Fouqué, P., Guglielmo, F., 1996, A&A 313, L21

Sánchez-Saavedra, M.-L., Battaner, E., Florido, E., 1990, MNRAS 246, 458

Sackett, P.D., 1997, ApJ 483, 103

Sancisi, R., 1976, A&A 53, 159

Sancisi, R., 1983, in: Internal Kinematics and Dynamics of Galaxies, IAU Symposium 100, ed. Athanassoula, E., Dordrecht: Reidel, p. 55

Sasaki, T., 1987, PASJ 39, 849

Sparke, L.S., Casertano, S., 1988, MNRAS 234, 873

Steiman-Cameron, T.Y., Kormendy, J., Durisen, R.H., 1992, AJ 104, 1339

Stein, P., 1996, A&AS 116, 203

van der Kruit, P.C., Searle, L., 1981a, A&A 95, 105

van der Kruit, P.C., Searle, L., 1981b, A&A 95, 116

van der Kruit, P.C., Searle, L., 1982a, A&A 110, 61

van der Kruit, P.C., Searle, L., 1982b, A&A 110, 79

Walker, I.R., Mihos, J.C., Hernquist, L., 1996, ApJ 460, 121